Development Roadmap and Preliminary Testing Results of a 250N Green Propellant Thruster

Duran Martin*†, Natalia Celeghini*, Hadeel AlNahdi*, Shaima Albedwawi*, Caique Presoto*, Fatema Alawadhi*,
Vito Salvatore*, Carmine Carmicino*, Henrique Argentieri*

*Propulsion and Space Research Centre – Technology Innovation Institute (TII) –

*PO Box: 9639 Masdar City, Abu Dhabi, UAE

duran.martin@tii.ae

† Corresponding Author

Abstract

This paper presents an overview of the development and testing of a 250 N thrust Nitrous Oxide/Propylene liquid rocket engine. Green propellants remain a subject of interest in the propulsion community due to their non-toxic nature, offering safer handling and reduced environmental impact compared to traditional storable propellants. Yet the challenge is to achieve performance comparable to standard hydrazine-based systems. Specific focus is on the injector, whose configuration was selected to be of the coaxial-swirling type. Subsequently, the engine hot-fire testing results are presented to assess its operational performance, combustion stability, and overall efficiency. Preliminary results indicate promising performance metrics, supporting the feasibility of N₂O/C₃H₆ as a viable green propellant combination for in-space propulsion systems.

1. Introduction

Over the past two decades we have witnessed a continuous and remarkable expansion of the small satellite market, driven by the rise of constellations and Low-Earth Orbit (LEO) applications [1]. Satellite miniaturization has significantly advanced, enabling the development of smaller, cost-effective CubeSats. These small satellites have opened opportunities for academic institutions, startups, and researchers to conduct space experiments and collect data at a fraction of traditional costs.

In today's evolving commercial space era, two main launch strategies are commonly employed for small satellites. The most frequent is the rideshare option, which involves using heavy launchers such as the SpaceX Falcon 9. The second is dedicated small or micro-launchers, a segment that is steadily growing, even though the launch's market share is dominated by the former [2].

Within this expanding field a new class of upper stages, known as Orbital Transfer Vehicles (OTVs), has emerged to enhance the capabilities of in-space missions. These platforms serve various roles, including last-mile payload delivery for spacecraft launched by heavy rockets, kick-stages for small launchers, and general on-orbit servicing [3]. In this context the search for green propellants to replace traditional hydrazine-based systems is a key focus. The toxicity of hydrazine and its derivatives is driving the propulsion community toward safer alternatives, such as non-toxic chemicals that deliver high specific impulse and ensure good propulsion performance, while minimizing environmental and health impacts across their lifecycle, including production, storage, transportation, and handling.

Targeting high specific impulse remains a key priority, as it provides the clear advantage of reducing the amount of propellant required for spacecraft maneuvers. This, in turn, enables an extension of satellite operational life. To illustrate the significance of this parameter, telecommunications satellites in geosynchronous orbit offer a good example. The reduced propellant mass enabled by higher specific impulse allows spacecraft to carry additional Attitude Control System (ACS) propellant or increase power generation capacity, both of which can directly enhance revenues for satellite operators. For scientific missions, the mass savings can instead be reallocated to expand the spacecraft's data collection capabilities, thereby increasing the scientific return.

Nitrous oxide (N₂O) and hydrogen peroxide (H₂O₂) are among the most promising storable green oxidizers. When coupled with light hydrocarbons, they offer good performance, that is comparable to unsymmetrical dimethylhydrazine (UDMH) and nitrogen tetroxide (NTO) systems, as well as storability, and ease of handling. Furthermore, both can be

utilized as monopropellant systems offering fair performance. The pros and cons shown by each of the two are analyzed in the following sections, where the selection of propellants is addressed.

This paper presents the liquid rocket engine development roadmap undertaken at the Technology Innovation Institute (TII) for in-space applications. The final objective to be achieved in 2026 is to modularly develop a 1 kN vacuum-thrust engine capable of long-duration burns (by being regeneratively cooled with nitrous oxide), following a two-phase approach: first, assess the combustion performance of a 250 N subscale version, and then scale up to the final target configuration. The monopropellant option is included in the overall development roadmap specifically for low thrust applications.

After the presentation of the roadmap in the forthcoming section, the rationale behind the design choices is introduced, followed by a discussion of the results gathered over the first hot-fire test campaign.

2. Liquid-Rocket Engine Development Roadmap and Basic Design Choices

Aligned with the national space initiatives for the period 2018–2030, driven by governmental (non-military), commercial, and scientific bodies across the public and private sectors, as well as academic institutions and R&D centres, one of the main objectives of the Propulsion and Space Research Centre (PSRC) of TII in Abu Dhabi (UAE) is to establish a hub for developing rocket propulsion capabilities in the UAE. This objective is being pursued by expanding its research activity with two projects related to the development of a sounding rocket powered by a hybrid rocket engine, and the development of a liquid propellant rocket engine for in-space propulsion. With reference to the latter, a phased approach is adopted. Accordingly, the liquid rocket engine program is divided into two main stages: 1. the development of a 1 kN thrust storable, bi-propellant liquid rocket engine for in-space propulsion applications to be carried out by the end of 2026. 2. progression (on a longer timeframe) toward the development of a cryogenic propellant engine for launcher stage propulsion.

The first stage, which is the focus of this paper, is further split into two phases. Initially, a 1/4-scale engine (250 N thrust) is developed for two primary purposes, i.e. to test the performance of the selected injector and determine the engine's characteristic length (L^*) allowing for reasonable combustion efficiency, and to develop a smaller thruster as a foundational step. The overall roadmap for these developments is depicted in **Figure 1**.

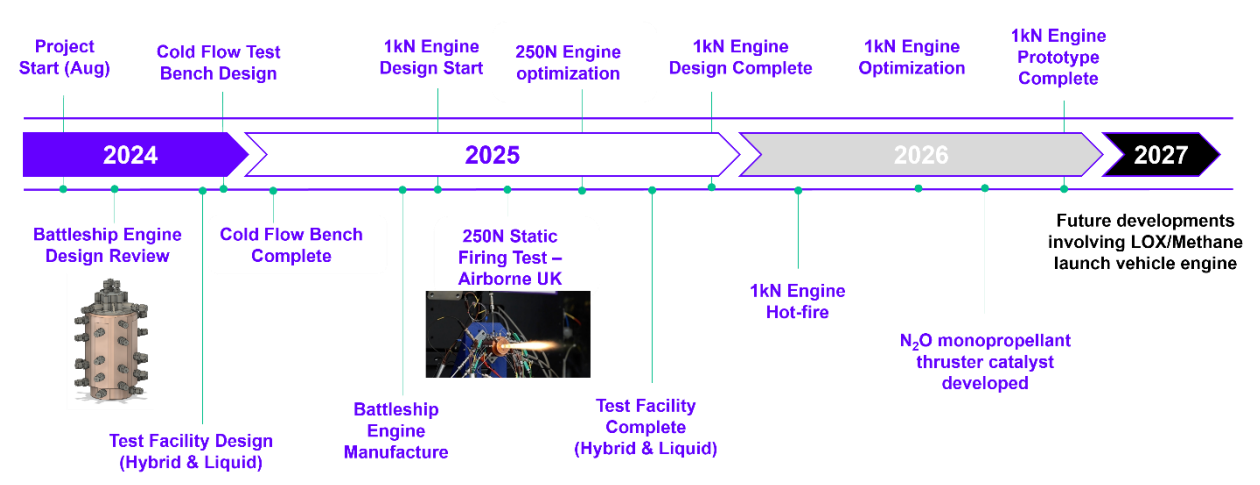


Figure 1: Liquid-rocket engine development program roadmap.

With reference to the picture above, we are in the stage of completion of the 250 N engine firing tests conducted in the test facility of Airborne Engineering Ltd, UK [4]. Note that PSRC is designing its own static fire test facility, which is expected to be operational by the end of the current year. On the same experimental facility, the 1 kN liquid propellant engine shall be tested, as well as the hybrid rockets developed in parallel to the current program.

The selection of the oxidizer between the two candidates mentioned above, i.e. hydrogen peroxide and nitrous oxide, has been made according to the following rationale. Although nitrous oxide delivers lower specific impulse and has lower density than hydrogen peroxide, it has significantly higher vapor pressure (around 50 bar at 20°C), a much lower freezing point, and superior long-term storability [5]. One of the main disadvantages of hydrogen peroxide is, indeed,

its high sensitivity to contamination, which can trigger a runaway decomposition reaction even with minor impurities. Additionally, hydrogen peroxide is compatible with only a limited range of materials, which complicates long-term storage. Thanks to the high vapor pressure of nitrous oxide, for applications not demanding the highest performance, it does not require any additional pressurizing system, which, upon selection of a fuel with similar vapor pressure (e.g. ethane), makes the design much simpler and cost effective [6].

Furthermore, it is non-corrosive and can be used with common materials; it is stable and practically unreactive at room temperatures. Hence, nitrous oxide appears to be a good compromise and has been selected as our oxidizer of choice. Note that, recently, bipropellant thrusters between 1 N and 200 N relying on the use of hydrocarbons with nitrous oxide have been extensively developed and tested at DLR's Institute of Space Propulsion in Lampoldshausen [7], as well as qualified by private companies and already flown in space (see the following sections). Nitrous Oxide can decompose exothermically following the chemical reaction in Eq. (1), reaching the adiabatic temperature of 1640 °C:

$$N_2O \to N_2 + 0.5O_2 + Heat$$
 (1)

where both the nitrous oxide and the reaction products (nitrogen and oxygen) are in the gaseous phase, and the rejected heat is equal to 82 kJ/mol. It should be noted that activating the decomposition thermally requires supplying about 250 kJ/mol of heat, that is approximately equivalent to heating up to 1000°C. The decomposition reaction can be accelerated through a catalyst, which offers operating nitrous oxide with lower activation barriers [8].

Taking advantage of the above-mentioned, the use of nitrous oxide can be extended to the monopropellant thruster application for low-thrust (few millinewtons) and up to-medium-thrust (500 N) in-space propulsion (e.g.: small satellites, CubeSats, small orbit maneuvers and spacecraft attitude control) [8]. As reported in the literature, noble metal-based catalysts such as Rhodium (Rh), Ruthenium (Ru), and Iridium (Ir) deposited on metal oxides such as γ -Al₂O₃, SiO₂, MgO, ZrO₂, TiO₂ and CeO₂ are commonly used for this purpose [9], [10].

The level of thrust for liquid rocket engines currently used for in-space propulsion varies widely depending on the mission type (e.g., satellite station-keeping, orbital transfer, deep space maneuvers) and propulsion system design. The thrust levels of the two selected systems (i.e. the 1 kN engine and its scaled version) are based on comparable engines currently in operation.

In fact, the 250 N engine falls within the typical range used for orbital maneuvering and orbital transfer platforms, such as the ATV 200 N thruster and the S400 pressure-fed liquid rocket engine developed by ArianeGroup [11]. The full-scale 1 kN engine occupies a distinct niche, delivering sufficient thrust for orbital maneuvers while remaining compact and suitable for smaller spacecraft or kick-stage missions. Comparable systems include the BT-4 pressure-fed engine developed by IHI Aerospace (Japan) [12] and the famous R-4D-15 HiPAT 445 N thruster produced by Aerojet Rocketdyne in the early 1960s for the Reaction Control Systems (RCS) for the Apollo Service Module and the Lunar Excursion Module [13].

With the thrust levels defined above, the chamber pressure has been decided according to the following considerations. On the one hand, when expanding to vacuum the specific impulse is only slightly increased by raising the chamber pressure, the main role being played by the nozzle expansion ratio; on the other hand, lower chamber pressure, for a given thrust level, implies larger rockets, simplifies the system thermal design, while reducing the need for turbopumps, and allowing for pressure-fed systems.

In **Table 1** a list of pressure-fed bipropellant thrusters produced by several manufacturers, all using either hydrazine-based or nitrous oxide/hydrocarbon fuel, is shown; also, data relative to a new throttleable engine using 98% hydrogen peroxide and 96% ethanol being developed in Poland are included [14]. Here, along with the thrust range, chamber pressure is reported. It is evident that all of them operate around 10 bar chamber pressure. Hence, 10 bar is our selected chamber pressure for the considered applications (both 250 N and 1 kN thrusters).

Engine	Pressure, bar	Propellants	Thrust, N	Notes
R-4D-15	9.4	MMH/NTO	445	Apollo Service Module RCS
IHI BT-4	10	MMH/NTO	500	H-II Transfer Vehicle (Japan)
SpaceX Draco	10-16	MMH/NTO	400	Dragon spacecraft
Aerojet Rocketdyne R-1E	7.3	MMH/NTO	111	Biprop maneuvering thruster
TLPD	10-15	HTP/Ethanol	5000	Throttleable engine demonstrator
Saiph thruster	7	N ₂ O/Ethane	22	Impulse Space Mira
B20-B200	$5-10^{a}$	N ₂ O/Propylene	18-200	Dawn Aerospace
HyNOx thruster	6	N ₂ O/Ethane	22	DLR

Table 1: Engines operating at chamber pressure close to 10 bar.

3. Engine Design Process

The design process began with propellant selection and performance prediction using NASA's Chemical Equilibrium with Applications (CEA) software [15], [16]. Nitrous oxide and propylene were selected as the oxidizer and fuel, respectively. A comparative study was conducted for the following candidate fuels: ethanol, propane, propylene, acetylene, and kerosene. Each option has been evaluated based on the specific impulse versus oxidizer-to-fuel mixture ratio (O/F). The analysis was performed under the following assumptions: vacuum conditions, chamber pressure of 10 bar, expansion ratio of 60, propellant temperature of 298 K, and frozen flow at the throat.

As shown in **Figure 2**, acetylene yields the highest specific impulse of all the alternative fuels; however, its instability at elevated pressures and concentrations, along with its tendency to produce excessively high chamber temperatures, poses safety and operational risks. In comparison to ethane, which is a good candidate for its high vapor pressure similarly to nitrous oxide (37.6 bar at 20°C), propylene offers several advantages in both performance and practicality. At 20°C, propylene is liquid with a density of approximately 515 kg/m³ [17], at the same temperature, the saturated liquid ethane density is approximately 358 kg/m³ [17], which is about 30% lower than that of propylene. The optimal O/F ratio for propylene is 6.7, compared to 7.9 for ethane, meaning propylene requires less oxidizer per unit of fuel mass, improving overall system balance. While the difference in vacuum specific impulse is relatively small, the combination of propylene's higher density, lower O/F ratio, and safer handling characteristics make it the preferred fuel. The propellant combination of nitrous oxide and propylene offers a balanced and practical solution, delivering good performance alongside safety, ease of handling, and availability. Propylene is non-toxic, has a relatively high specific impulse (estimated at 302 seconds in vacuum with the modest expansion ratio of 60), a low freezing point of -185 °C, and a predicted chamber temperature of approximately 3250 K.

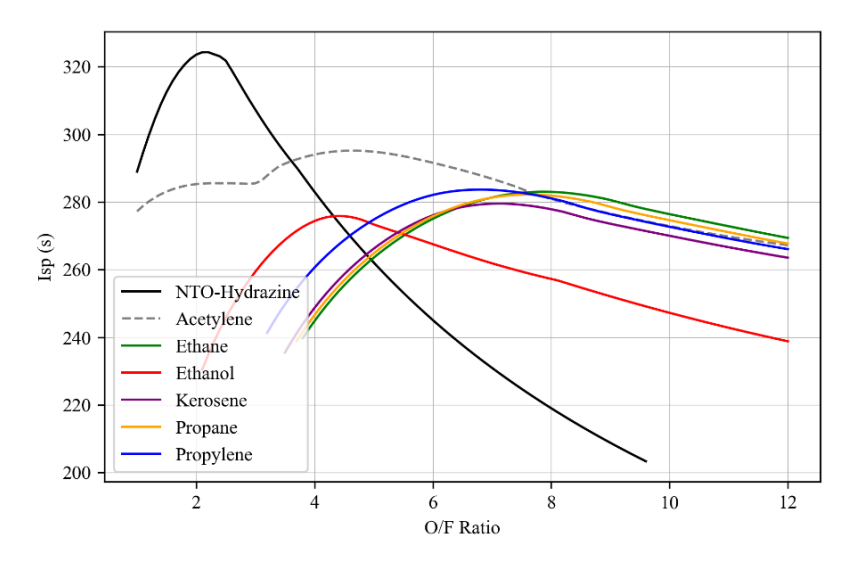


Figure 2: Comparison of specific impulse for different fuels with N₂O at varying O/F ratios

^aEstimated from the available performance data

Based on the above-mentioned results, the engine design parameters were set to a chamber pressure of 10 bar, an expansion ratio of 60, and a vacuum thrust of 250 N, with an O/F ratio of 6.7. The engine is expected to deliver approximately 168 N of thrust at sea level. Additional performance targets include achieving a combustion efficiency of \geq 95%, and withstanding flame temperatures up to 3000 K.

3.1 Injector design

A single element injector design was selected so that the injector, once optimized, can be scaled to the larger 1 kN engine by increasing the number of injection elements under the same operating conditions. Additive manufacturing was employed to enable complex and optimized designs, while reducing the manufacturing and assembly requirements of the engine. However, surface roughness and the associated pressure losses need to be managed with this manufacturing process. Of the different injector types, coaxial and swirl type injectors are typically employed in additively manufactured injectors as the element geometry requires little modification to be compatible with this process. **Figure 3** shows a classical swirl element design for a single propellant with reference to the critical dimensions used in the design process.

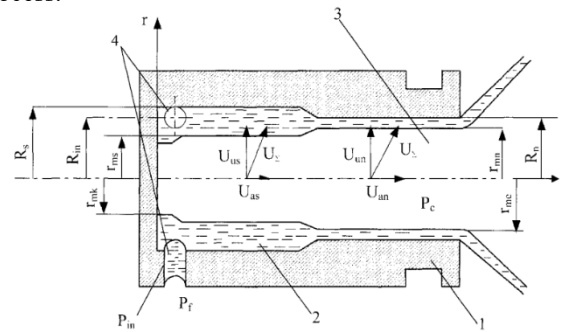


Figure 3: Single swirl element configuration [18].

The methodology developed by Bazarov [18] was utilized to design a coaxial swirl injector. In this methodology, three dimensionless parameters are used: the geometric characteristic parameter A, coefficient of passage fullness, φ , and discharge coefficient, μ . The geometric characteristic parameter A is shown in Eq. (2), where R_n is the nozzle radius, R_{in} is the inlet orifice radial position, and r_n is the inlet orifice radius. A is proportional to the spray angle, and inversely proportional to the injector discharge coefficient.

$$A = \frac{R_n R_{in}}{r_{in}^2} \tag{2}$$

Based on the relatively low flow rate of propylene compared to nitrous oxide, propylene was selected as the inner swirl element to maintain a reasonable discharge coefficient. The two-phase flow of nitrous oxide was simplified by using the Homogenous Equilibrium Model (HEM) [19]. As a starting point, the targeted pressure drop (ΔP), mass flow rate (\dot{m}), and density (ρ) where used in Eq. (3), to determine the resulting nozzle radius. An initial, targeted spray angle was assumed to estimate the corresponding discharge coefficient. Other parameters such as inlet orifice diameters are constrained by manufacturing processes.

$$R_n = 0.475 \sqrt{\frac{\dot{m}}{\mu \sqrt{\rho \Delta P}}} \tag{3}$$

Pressure losses are accounted for across the orifice inlets and as a friction factor for the wetted surface of the swirling element using the Blasius correlation for the Darcy-Weisbach equation. Here the surface roughness corresponds to the as-printed surface. An equivalent geometric characteristic parameter is then calculated based on these losses, as per **Eq. (4)**, from which the equivalent discharge coefficient, μ_{eq} , can be determined. The orifice loss coefficient, ξ_i , is used to calculate the actual discharge coefficient, μ_{ij} , shown in **Eq. (5)**.

$$A_{eq} = \frac{R_{in}R_n}{nr_{in}^2 + \frac{\lambda}{2}R_{in}(R_{in} - R_n)} \tag{4}$$

$$\mu_{i} = \frac{\mu_{eq}}{\sqrt{1 + \xi_{i} \mu_{eq}^{2} \frac{A^{2}}{\bar{R}_{in}^{2}}}}$$
 (5)

The updated nozzle radius is then calculated based on actual flow coefficient, as per Eq. (3), and the process is iterated until the parameters converge. Both swirl elements for the fuel and oxidizer are designed together, such that the outer wall of the inner coaxial element is smaller than the expected fluid film diameter of the outer element, such that the one can be located inside the other in the traditional, coaxial swirl injector configuration. Given the uncertainty of the effect of surface roughness, fluid properties, manufacturing quality on the overall pressure drop, multiple designs were considered with varying inlet orifice configurations.

The primary injector manifold was additively manufactured from Inconel 718, with interchangeable brass inserts to enable different inner swirl element designs for propylene. Three additively manufactured manifolds, each with variations in the number and size of the inlet orifices were printed, along with a multitude of propylene swirl inserts also with varying inlet orifices, and varying lengths to adjust the overall recess length of the element.

3.2 Combustion Chamber Design

The combustion chamber is a critical component in a liquid rocket engine, responsible for providing sufficient volume to ensure propellant mixing and complete combustion upstream of the nozzle where the resulting high temperature gases are accelerated to generate thrust. The chamber must withstand the extreme thermal and pressure conditions associated with the combustion process while maintaining structural integrity and meeting performance targets.

The characteristic length (L^*) is a critical parameter in combustion chamber design, reflecting the volume-to-throat area ratio and influencing combustion efficiency. A review of relevant literature was conducted to assess typical L^* values for engines operating with nitrous oxide. Based on this review, **Table 2** was developed to summarize L^* ranges observed for various fuels. These values were used to guide the selection of L^* in the design of the chamber configurations evaluated in this study.

Table 2: Characteristic Length for Propellant Combinations including N2O Based on Literature Sources

Propellants	Thrust, N	L*, m	Ac/At	Reference
N ₂ O + Propane	350	$2 \le L^* \le 3$	4.4	[20]
$N_2O + Ethanol$	3000	$1.25 \le L^* \le 3$	3.82	[21]
$N_2O + RP-1$	3000	$1.14 \le L^* \le 1.32$	3.82	[21]
$N_2O + Ethane$	3000	~ 1.05	9	[22]
N ₂ O monopropellant	1	1	-	[23]
N ₂ O + Ethylene (gaseous & pre-mixed)	-	$0.79 \le L^* \le 1.71$	7.11	[24]

To investigate the effects of geometric parameters on performance and thermal behavior, multiple chamber configurations were developed. As shown in **Table 3**, two contraction ratios (10 and 15) were considered. For each contraction ratio, chambers were designed with different characteristic lengths (L*): 0.8 and 1.2 m for contraction ratio of 10, and 1.2 and 2.0 m for contraction ratio of 15. These configurations were analyzed to assess their impact on combustion efficiency and thermal loading.

Configuration	Contraction Ratio	L*, m
1	10	0.8
2	10	1.2
3	15	1.2
4	15	2.0

Table 3: Combustion Chamber Configurations

To determine the appropriate wall thickness of the combustion chamber, a thermal analysis was conducted to predict the temperature distribution through the chamber wall during firing. The goal was to estimate the thermal load on the inner wall surface and determine the temperature gradient through the material, which directly affects the minimum required thickness to avoid overheating or structural failure. The analysis followed a multi-step approach: initial conditions and design data were extracted from CEA, followed by calculation of local heat transfer coefficients and wall temperatures using the Bartz equation.

The thermal model considers gas-side heat transfer, which occurs by forced convection from the combustion gases to the chamber wall. As described in [25], heat transfer across the boundary layer can be expressed using the following relation:

$$q = h_g \left(T_{aw} - T_{wg} \right) \tag{6}$$

Where q, h_g , T_{aw} and T_{wg} are heat flux, gas-side-heat transfer coefficient, adiabatic wall temperature and hot-gas-side local chamber wall temperature, respectively. The adiabatic wall temperature was calculated using the following relation, which accounts for the compressible boundary layer effects:

$$T_{aw} = T_o \left[\frac{1 + r\left(\frac{\gamma - 1}{2}\right) M_x^2}{1 + \left(\frac{\gamma - 1}{2}\right) M_x^2} \right]$$
 (7)

Where T_o , M_x , r denote nozzle stagnation temperature, local Mach number and local recovery factor, respectively. The heat transfer coefficient h_g was calculated using the Bartz equation, widely used for estimating convective heat transfer in rocket engines. The local recovery factor r was estimated based on the Prandtl number using the empirical relation $r = Pr^{0.33}$, assuming turbulent flow. The expression used to compute h_g is given as follows:

$$h_g = \left[\frac{0.026}{D_t^{0.2}} \left(\frac{\mu^{0.2} C_p}{P r^{0.6}} \right) \left(\frac{P_c}{c^*} \right)^{0.8} \left(\frac{D_t}{R} \right)^{0.1} \right] \left(\frac{A_t}{A} \right)^{0.9} \sigma$$
 (8)

$$\sigma = \frac{1}{\left[\frac{1}{2}\frac{T_{wg}}{T_o}\left(1 + \frac{\gamma - 1}{2}M^2\right) + \frac{1}{2}\right]^{0.68}\left[1 + \frac{\gamma - 1}{2}M^2\right]^{0.12}}$$
(9)

The geometric parameters D_t , A_t , A and R correspond to the diameter at the throat, the area at the throat, the local cross-sectional area and nozzle radius of curvature at throat, respectively. The terms P_c and c^* denote the chamber pressure and characteristic velocity. Meanwhile, σ is a correction factor for property variations across the boundary layer and it varies as a function of the wall temperature T_{wg} , which is initially unknown. To address this, an iterative procedure was applied: T_{wg} was first assumed and used to compute σ , and subsequently, the resulting wall temperature was extracted from the thermal analysis in ANSYS. This updated T_{wg} was then used to recalculate σ in the next iteration. The process was repeated until convergence was achieved, ensuring consistency between the heat transfer coefficient and the wall temperature boundary condition. This methodology was implemented to generate axial distribution of h_g and T_{aw} , which were then used as input boundary conditions in a transient thermal analysis in ANSYS. The convective heat flux q was applied on the inner wall surface, while natural convection was applied to the outer surface. The results

were analyzed considering the thermal properties of copper to assess material response and thermal loading under representative operating conditions.

As illustrated in **Figure 4**, these outputs provide insight into the thermal behavior of the chamber. The analysis was conducted over several firing durations (5, 10, and 15 seconds), and the required wall thickness was conservatively determined based on maintaining the largest wall temperature (attained in the nozzle throat region) below the material's allowable limit, while also considering manufacturing constraints and the integration of instrumentation ports. Thermocouple ports and pressure ports were incorporated into the chamber design to enable experimental validation of thermal analysis. The collected data will be used to assess the accuracy of the simulation results. Details of the instrumentation layout and corresponding results will be presented in future work. The complete assembly of the 250N engine is shown in **Figure 5**.

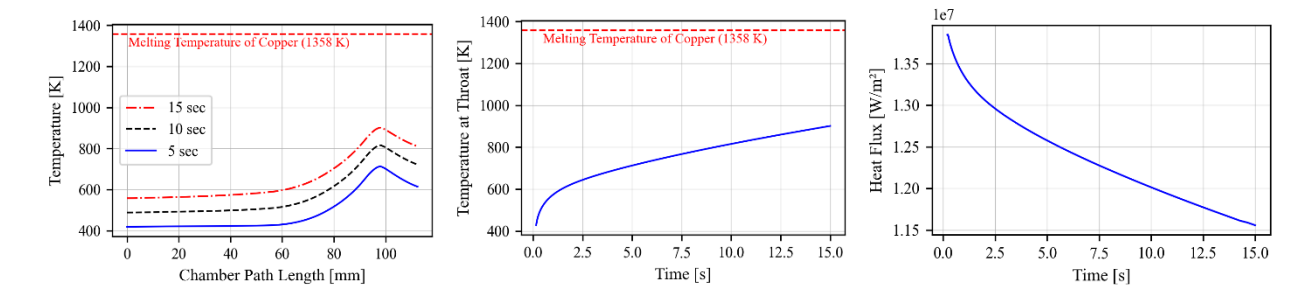


Figure 4: Simulated Chamber Inner Wall Temperature at Different Time Intervals, Throat Temperature and Radial Heat Flux Profile Distribution Over Time.



Figure 5: Assembled 250 N engine.

4. Test Rig Schematics and Operation

The first firing test campaign of the 250 N thruster has been carried out at the Westcott rocket test facility (UK) operated by Airborne Engineering [26]. The test stand was used in a blow-down, pressure-fed configuration, shown in **Figure 6**. Both propellant tanks were supercharged with nitrogen to maintain constant tank pressure during tests and achieve relatively constant conditions in the engine. The mass flow rate was measured using Coriolis flow meters, and temperature and pressure were measured both upstream and downstream of the throttle valve, as well as directly before the injector inlet. In the injector manifold, pressure and temperature are also measured to get a close representation of the properties at the inlet of the injection element, and pressure drop across the injector.

The targeted flow rate was achieved by using active, open-loop control of the main throttle valve, correcting the valve position based on a calibrated valve coefficient coming from cold-flow tests. This proved reliable and consistent, where the difference between the targeted and achieved flow rate was typically less than ± 0.3 g/s and ± 1 g/s for propylene and nitrous oxide respectively.

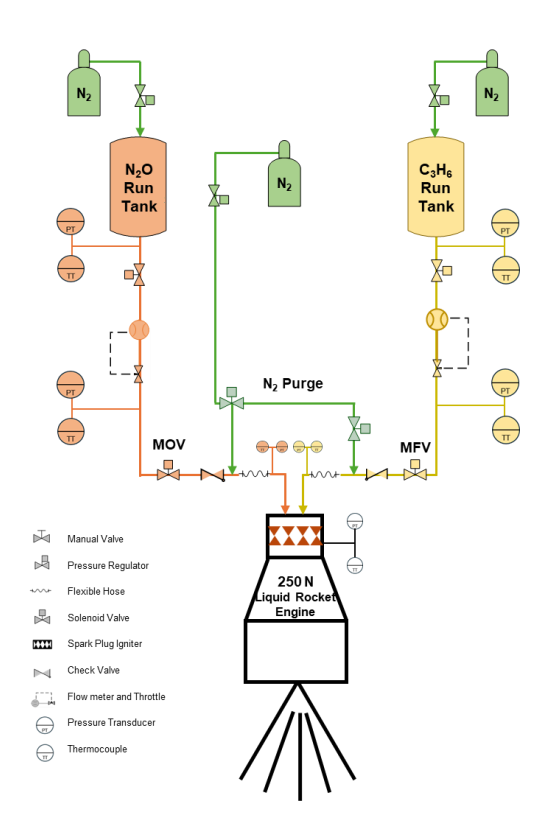


Figure 6 :Simplified P&ID of the N₂O/C₃H₆ test stand.

Figure 7 shows the hot firing test sequence of the engine. The startup sequence was defined based on a series of cold flow tests to offset the delays between the feed valves. To ensure the cleanliness of the lines from any residual propellants, the sequences started by simultaneous nitrogen gas (N_2) purge to the fuel and oxidizer lines. It was followed by the propellants feed at 100% of the nominal mass flow rate and ignited at t=0 for 1 second. It should be noted that the test durations varied between 7 s, 15 s or 20 s depending on the tested engine configuration. To ensure safe shutdown of the engine, the flame was extinguished by opening the $Ox-N_2$ purge valve and blowing out the oxidizer through the injector. Then, the fuel was flushed on two segments through the injector by opening the $FUL-N_2$ purge valve while keeping the $Ox-N_2$ purge valve open to continue chilling down the engine and to avoid the re-ignition risk.

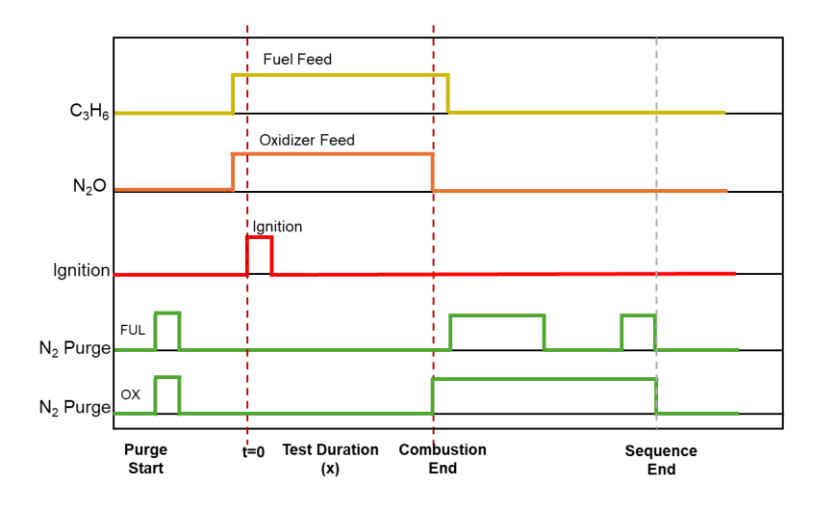


Figure 7: N₂O/Propylene engine hot-firing test sequence.

Engine ignition was achieved using a spark plug actuated through a custom-designed electrical circuit. The system operates with 220 V AC, 50 Hz main power supply, which feeds a two-stage voltage transformation setup. The first

transformer steps down the line voltage from 220 V to 120/110 V to match the input requirements of the subsequent high-voltage transformer. This second stage utilizes a Honeywell Q624A1014 Solid State Ignition Transformer, chosen for its reliability, suitability for intermittent ignition demands, and commercial availability. The high-voltage transformer then steps up the voltage to approximately 10,000 V, which is delivered to the ignition element, an NGK 6482 CR10EIX Iridium IX spark plug. The system follows a normally OFF configuration, with the ON state controlled by a solid-state (SS) relay rated for a 3–32 V DC control input. This relay is triggered via an auxiliary control circuit powered by an external DC source, which includes a 1 k Ω current-limiting resistor to ensure safe operation of the relay.

5. Static Hot-Fire Tests Results

Over 50 hot-fire tests were conducted over a week-long campaign (see **Figure 8**). Multiple configurations of injector and combustion chambers were tested, and a wide range of engine performance parameters were explored. In the following, some basic preliminary results gathered from the firings are reported.



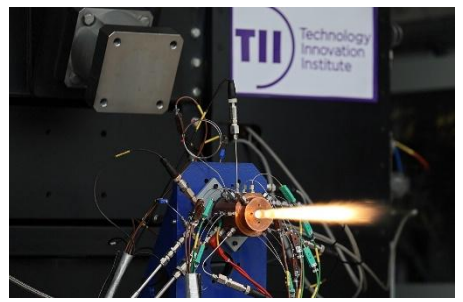


Figure 8: Static hot-fire test of the 250 N engine.

Some noteworthy configurations and the relevant results are shown in **Table 4**, where the measured c^* has maximum uncertainty of $\pm 2.85\%$ when accounting for error in mass flow rate, pressure and nozzle geometric measurements. The injector configuration uses a 3-digit identification code, where the first digit indicates which additively manufactured manifold and nitrous oxide configuration was used. The second digit identifies which type of propylene insert was used with respect to the inlet orifices. The third digit gives a relative length of the propylene insert, which is inversely proportional to the recess length of the coaxial element.

Table 4: Combustion efficiency for different injectors and chamber configurations

Injector Configuration ID	Contraction Ratio	L*, m	Throttle, %	C* Efficiency, %
118	15	2.0	100	94.0%
118	15	2.0	111	92.1%
118	10	0.8	100	87.9%
118	10	0.8	110	86.0%
217	10	0.8	101	83.5%
217	10	0.8	115	73.8%
319	10	1.2	99	86.9%
319	10	1.2	120	92.7%
326	15	2.0	100	88.3%
326	15	2.0	115	91.1%

Injector configuration 118 was the highest performing injector, at an average combustion efficiency of 94%. Increasing the flow rate did not increase performance. Decreasing L* for this configuration resulted in a reduction in performance. Injector configuration 217 was the lowest performing configuration of the test campaign. When coupled with the

smallest combustion chamber and an above nominal flow rate, it produced the lowest efficiency of 73.8%. Other configurations showed moderate performance (80-90%) but typically an increase in performance is observed when increasing the flow rate in the larger chambers.

Depending on the temperature of propylene, chamber pressure, and pressure drop through the inner injector, coupling was hypothesized to occur between the chamber pressure and phase change of propylene. The increase in flow rate, resulting in an increase in chamber pressure, is believed to raise the chamber pressure above the saturation pressure of the propylene, where the injector would then operate as designed. This is most notably seen with configuration 319 in a mid-sized chamber, which achieved 86.9% at nominal flow rates, but increased to 92.7%, at an increased flow rate of 20%.

In the specific test shown in **Figure 9**, the combustion is highly unstable, fluctuating between distinct stable and unstable modes. During the brief moments of stability, the performance is nominal, where the injector is behaving as expected. However, as the chamber pressure fluctuates below the saturation pressure of the liquid propylene, and as the injector and propylene heat up, phase change occurs in the injector triggering a low-frequency (around 200 Hz), non-acoustic, non-destructive instability with peak-to-peak amplitudes up to 39% of the mean pressure.

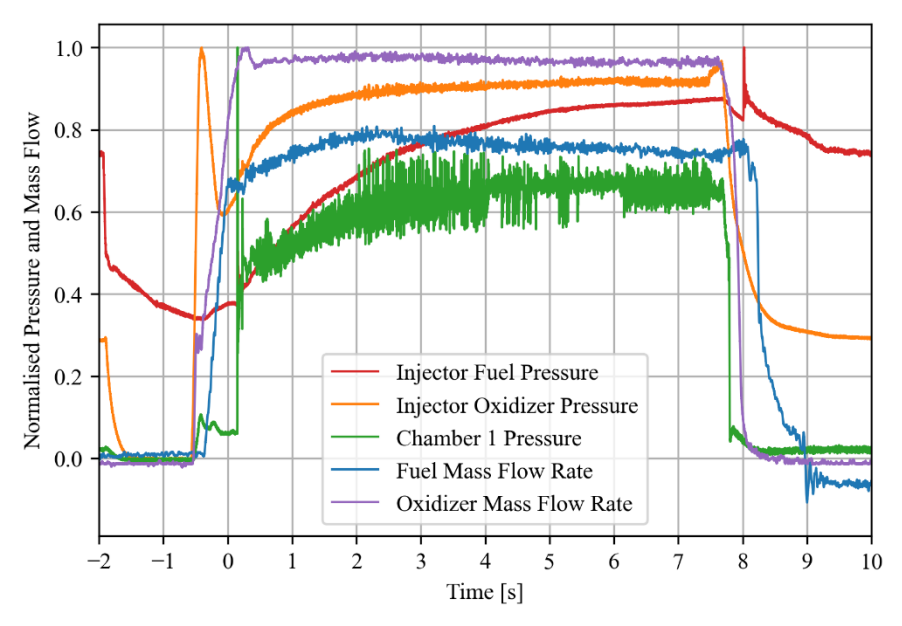


Figure 9: Hot-fire data for an unstable engine configuration

By changing the injector configuration, stable combustion was achieved with peak-to-peak values of no greater than 2% of the mean (see **Figure 10**). The ignition was most reliable and repeatable when the valves were opened with a slight lead such that the propellant mass flow rate was at nominal conditions at T-0. This would result in an accumulation of propellants in the chamber prior to ignition, where a notable pressure spike occurs on startup. The engine was designed with sufficient safety margin such that this was not a concern throughout the test campaign. For flight-weight configurations, refinement of the startup sequence is required to manage the over-pressure on ignition and reduce wasted propellant.

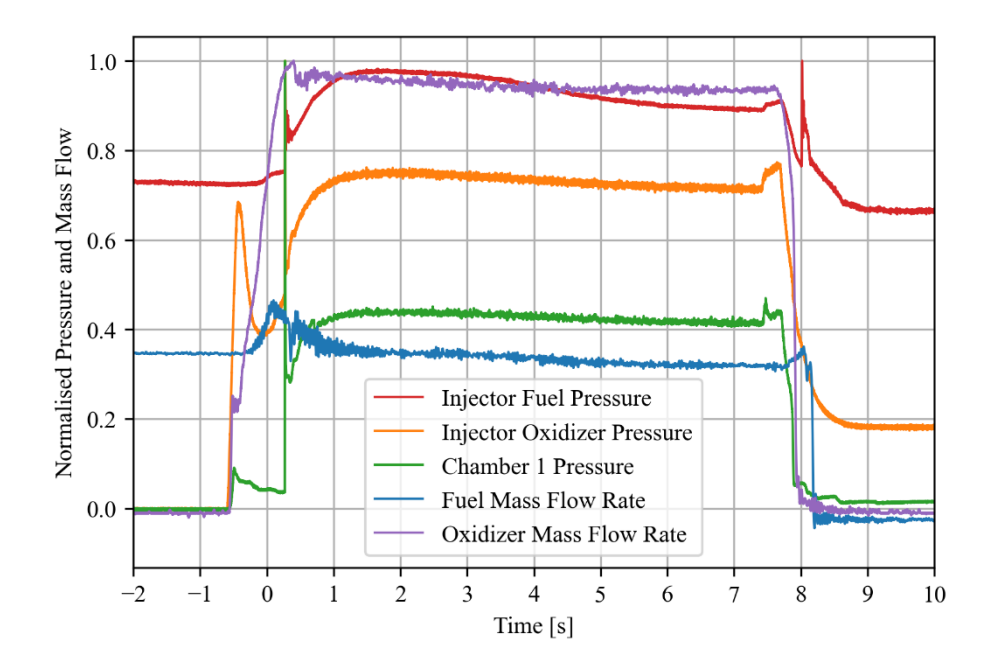


Figure 10: Hot-fire data showing nominal performance

6. Conclusions

This paper presented the development roadmap of the liquid rocket engine program at TII and preliminary hot-fire testing of a 250-N storable green bipropellant thruster utilizing nitrous oxide and propylene. The selected coaxial swirl injector configuration, designed with scalability in mind, demonstrated promising combustion efficiencies of up to 94%, validating both the injector design methodology and the propellant combination, but at the same time highlighting the need for further improvement and consequent testing. Extensive testing across multiple chamber geometries and injector variants provided insights into the effects of L*, contraction ratio, and flow rate on combustion stability and performance.

Observed dependencies between injector performance and propylene phase behavior underscore the importance of controlling feed conditions, particularly under sub-saturation chamber pressures. The successful demonstration of stable, efficient combustion across a range of configurations confirms the viability of this architecture for in-space propulsion applications. These results support the continuation of the development roadmap toward a regeneratively cooled 1-kN class engine, reinforcing nitrous oxide/propylene as a credible and safer alternative to legacy storable propellants.

7. References

- [1] BryceTech, "Smallsats by the Numbers," 2025. [Online]. Available: https://brycetech.com/reports/report-documents/smallsats-2025/
- [2] E. Kulu, "Small Launchers 2023 Industry Survey and Market Analysis," vol. 8, no. October, pp. 2–6, 2023.
- [3] A. Sarritzu and A. Pasini, "Performance comparison of green propulsion systems for future Orbital Transfer Vehicles," *Acta Astronaut.*, vol. 217, no. January, pp. 100–115, 2024, doi: 10.1016/j.actaastro.2024.01.032.
- [4] "Airborne Engineering." https://www.ael.co.uk/
- [5] S. Carlotti and F. Maggi, "Evaluating New Liquid Storable Bipropellants: Safety and Performance Assessments," 2022.
- [6] M. Perry, A. Hunt, and S. Christian, "Ground Test Development of 800lbf Nitrous Oxide-Ethane Bipropellant Engine," in *AIAA Propulsion and Energy 2020 Forum*, doi: 10.2514/6.2020-3789.
- [7] L. Werling *et al.*, "From Lampoldshausen to Space: DLR Spin-off InSpacePropulsion Technologies and the Development Status of Green Propellant Thrusters Based on H 2 O 2 and N 2 O," 2023, doi: 10.13009/EUCASS2023-596.
- [8] V. Zakirov, P. M. Sweeting, T. Lawrence, and J. Sellers, "Nitrous Oxide as a Rocket Propellant," *Acta Astronaut.*, vol. 48, no. 5, pp. 353–362, 2001.

- [9] X. Wu *et al.*, "Progress and challenges in nitrous oxide decomposition and valorization," *Chem. Soc. Rev.*, pp. 8379–8423, 2024, doi: 10.1039/d3cs00919j.
- [10] M. Konsolakis, "Recent Advances on Nitrous Oxide (N 2 O) Decomposition over Non-Noble-Metal Oxide Catalysts: Catalytic Performance, Mechanistic Considerations, and Surface Chemistry Aspects," 2015, doi: 10.1021/acscatal.5b01605.
- [11] "200N Birpropellant Thrusters, Orbital Propulsion Centre, Lampoldshausen, Germany." https://www.space-propulsion.com/spacecraft-propulsion/bipropellant-thrusters/200n-bipropellant-thrusters.html
- [12] IHI Aerospace Co. Ltd., "Bipropellant Thrusters," Japan. [Online]. Available: www.ihi.co.jp/ia/en
- [13] Aerojet Rocketdyne, "In-Space Propulsion Data Sheets Monopropellant Propulsion," Redmond, Washington, USA.
- [14] A. Okni, "On development of green storable liquid rocket engine with thrust variation," *Acta Astronaut.*, vol. 234, no. May, pp. 560–574, 2025, doi: 10.1016/j.actaastro.2025.05.020.
- [15] S. Gordon and J. Mcbride, "Computer program for calculation of complex chemical equilibrium compositions and applications. Part 1: Analysis," 1994.
 [16] B. J. Mcbride and S. Gordon, "Computer Program for Calculation Complex Chemical Equilibrium
- [16] B. J. Mcbride and S. Gordon, "Computer Program for Calculation Complex Chemical Equilibrium Compositions and Applications II. Users Manual and Program Description," 1996.
- [17] "NIST Chemistry WebBook. Thermophysical Properties of Fluid Systems," *National Institute of Standards and Technology*.
- [18] V. Bazarov, V. Yang, and P. Puri, "Design and Dynamics of Jet and Swirl Injectors," in *Liquid Rocket Thrust Chambers: Aspects of Modeling, Analysis and Design*, in Progress in Astronautics and Aeronautics, vol. 200. Reston ,VA: American Institute of Aeronautics and Astronautics, 2004, pp. 19–103. [Online]. Available: https://arc.aiaa.org/doi/book/10.2514/4.866760
- [19] J. Dyer, G. Zilliac, A. Sadhwani, A. Karabeyoglu, and B. Cantwell, "Modeling Feed System Flow Physics for Self-Pressurizing Propellants," in 43rd AIAA/ASME/SAE/ASEE Joint Propulsion Conference & Exhibit, doi: 10.2514/6.2007-5702.
- [20] R. Herdy, "Nitrous Oxide/Hydrocarbon Fuel Advanced Chemical Propulsion: DARPA Contract Overview".
- [21] T. Palacz, "Nitrous Oxide Application for Low Thrust and Low Cost Liquid Rocket Engine," 2017, doi: 10.13009/EUCASS2017-474.
- [22] M. A. Shelton and J. P. Biaglow, "Development of a Self-Pressurizing Ethane-Nitrous Oxide Propulsion System for an Amateur Rocket," 2018. [Online]. Available: https://api.semanticscholar.org/CorpusID:52831185
- [23] T. Hörger, F. Merz, J. Steelant, L. Werling, and C. Kirchberger, "Result of ESA-Greenraim Test Activities Part 2: Experimental Investigation of a 1 Newoton Nitrous Oxide Monopropellant Research Thruster," 2024.
- [24] L. Werling, T. Hörger, H. Ciezki, and S. Schlechtriem, "Experimental and Theoretical Analysis of the Combustion E ffi ciency and the Heat Loads on a N 2 O / C 2 H 4 Green Propellant Combustion Chamber," 2019, doi: 10.13009/EUCASS2019-142.
- [25] H. Huzel, D. K., Huang, D. H., & Arbit, Modern engineering for design of liquid-propellant rocket engines. American Institute of Aeronautics and Astronautics (AIAA), 1992.
- [26] I. Waugh, E. Moore, A. Greig, J. Macfarlane, and A. Watts, "Overview of Rocket Testing at the Westcott Test Facility (2021)," no. May, 2022.